# A Chiral Sensor Array for Peptidoglycan Biosynthesis Monitoring Based on MoS$_2$ Nanosheet-Supported Host−Guest Recognitions
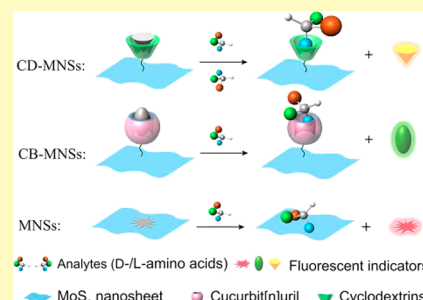
Feng Zhang, Chenwei Lu, Min Wang, Xinsheng Yu, Weili Wei,*[ORCID] and Zhining Xia

School of Pharmaceutical Sciences and Innovative Drug Research Centre, Chongqing University, Chongqing 401331, PR China

S Supporting Information

**ABSTRACT:** Monitoring the dynamic change with respect to chirality and species of amino acids in bacterial peptidoglycan (PG) during cell wall biosynthesis is correlated with bacterial taxonomy, physiology, micropathology, and antibacterial mechanisms. However, this is challenging because reported methods usually lack the ability of chiral analysis with the coexistence of D- and L-amino acids in PG. Here we report a chiral sensor array for PG biosynthesis monitoring through chiral amino acid recognition. Multitypes of host molecule modified MoS$_2$ nanosheets (MNSs) were used as receptor units to achieve more accurate and specific sensing. By applying indicator displacement strategy, the distinct and reproducible fluorescence-response patterns were obtained for linear discriminant analysis (LDA) to accurately discriminate achiral Gly, 19 L-amino acids and the corresponding 19 D-enantiomers



simultaneously. The sensor array has also been used for identifying bacterial species and tracking the subtle change of amino acid composition of PG including chirality and species during biosynthesis in different growth status and exogenous D-amino acid stimulation.

**KEYWORDS:** chiral sensor array, host−guest chemistry, MoS$_2$ nanosheets, amino acid, peptidoglycan, biosynthesis

Peptidoglycan (PG) is an essential polymer in the bacterial cell wall composed of linear glycan strands cross-linked by short peptides. The glycan moiety of the PG is remarkably uniform.[1] However, the composition including the chirality and types of amino acids in PG's peptide varies significantly among different bacterial species,[2] growth phases,[3] and environment such as stimulation of high ionic stress,[4] exogenous amino acids,[5,6] and antibiotics.[7] In all known organisms, amino acids are predominantly synthesized and used as their L-enantiomers while PG is a rare exception that natively contain D-amino acids. The D-Ala and D-Glu are the most common D-amino acids present in PG. Sometimes, other D-amino acids such as D-Met, D-Leu, D-Tyr, and D-Phe are also synthesized and incorporated into PG with the change of growth condition, which helps bacteria adapt to environmental challenges.[8] Therefore, dynamic monitoring of the amino acid species and chirality of PG play important roles in bacterial taxonomy,[1] physiology,[9,10] micropathology,[11] and understanding of antibacterial mechanism.[12] Until now, high-performance liquid chromatography (HPLC)[13] and nuclear magnetic resonance spectroscopy[3] are the most general methods for PG composition analysis, and atomic force microscopy (AFM)[14] and cryo-electron tomography[15] have been used to provide morphological insights of PG architecture. They are powerful but usually time-consuming, and require trained personnel and expensive instruments which greatly limit their widespread application. Most importantly, they usually lack the ability of chiral analysis considering the coexistence of D- and L-amino acids in PG. Therefore, a high-throughput sensing method for chiral analysis

of PG's amino acid composition with convenient instruments is important but remains unexplored.

Recently, the sensor arrays have emerged as a novel powerful tool for identifying a wide range of analytes from small molecules[16] to macromolecules[17] and even cells.[18,19] These arrays follow a hypothesis-free signature-based strategy[20] that allows them to be particularly suitable for real analytes with complex matrices such as environmental,[21] clinical,[22] and biological samples.[23] However, identification of analytes in reported arrays mainly relies on the recognition of conventional physicochemical properties (i.e., molecular size, polarity, and charge), which may not be sufficient for the subtle conformational or enantiomeric differences. There is therefore a need to develop a sensor array with new recognition strategy for more subtle molecular differences. Host−guest chemistry[24] based on macrocyclic hosts has been found to be a powerful molecular recognition mode and widely used in sensors,[25] smart drug delivery,[26] and so on. The host molecules are focusing on recognition of specific molecular moieties. For instance, the cyclodextrins (CDs) differentiate hydrophobic groups with respect to chirality, polarity, and size,[27,28] while cucurbit[n]uril (CB[n]) has a different recognition strategy to guest molecules that contain both cationic and nonpolar moieties.[29] Thus, construction of sensor arrays by combining different types of host−guest interactions is expected to achieve more accurate and specific differentiation of analytes. However, this strategy
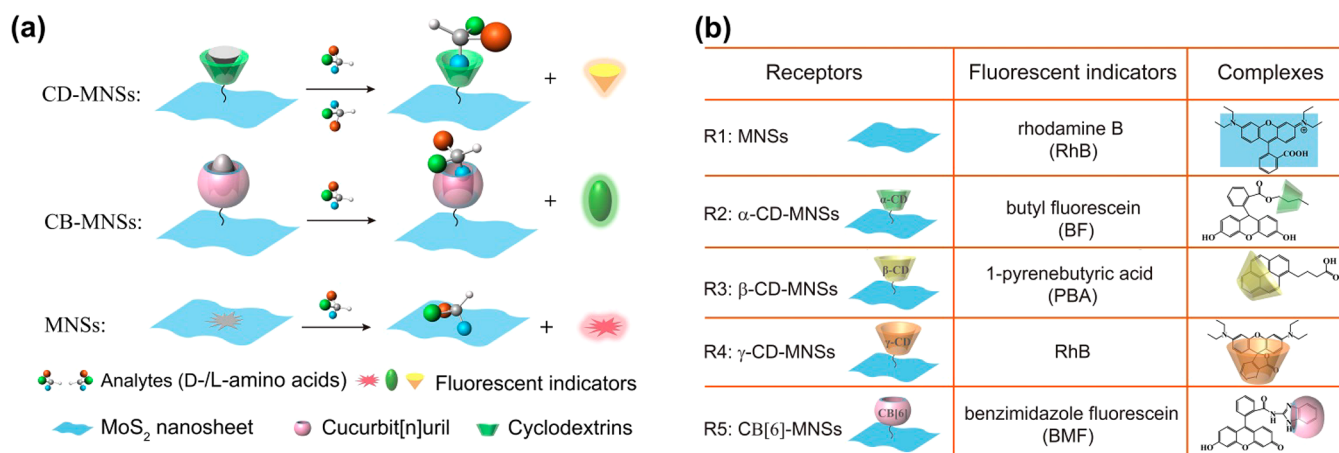
**Figure 1.** Schematic illustration of fabrication of a chiral sensor array based on multitypes of host molecule-modified MNSs for monitoring PG biosynthesis. (a) Illustration of the competitive interaction between analytes and fluorescent indicators with host molecules, which leads to fluorescence intensity change. (b) Receptor units of the sensor array and corresponding fluorescence indicators as well as their complexes.

has never been applied to sensing in challenging complex matrix, such as PG.

Herein, we design a novel chiral sensor array based on multitypes of host−guest recognition for PG biosynthesis monitoring (Figure 1). The novel two-dimensional MoS₂ nanosheets (MNSs) are used as scaffolds of host molecules to construct receptor units of the array. We use MNSs because of following reasons: (1) MNSs can quench nearby fluorophores[30] allowing transduction of recognition events into fluorescent signals; (2) MNSs have high specific surface area which provide more binding sites;[31] (3) the ready formation of Mo−S bonds[32] enable the easy linking of host molecules to them; (4) pristine MNSs can also serve as receptors.[31] As shown in Figure 1a, three types of receptors including CD-modified MNSs (CD-MNSs), CB[6]-modified MNSs (CB-MNSs), and pristine MNSs are designed for recognition of chiral hydrophobic moieties, nonpolar cationic moieties, and conventional physiochemical properties, respectively. Each receptor associated with corresponding fluorescent indicators to produce quenched complexes (Figure 1b). The subsequent recognition of analytes displaces the indicators, recovering the fluorescence. The receptor−indicator arrays render distinct fluorescent response fingerprints for an analyte (i.e., amino acid and PG). This sensor array does not require special instruments, and its sensitivity (due in large part to the ultrahigh specific surface area provided by the MNSs), selectivity (due to the specific recognition ability provided by host−guest chemistry), and speed facilitate simultaneous chiral analysis of amino acids and monitoring of PG biosynthesis.

## ■ EXPERIMENTAL SECTION

**Materials.** All chemicals, unless specified otherwise, were purchased from Sigma-Aldrich and used as received. Standard amino acids were purchased from Daicel Chiral Technologies (China) Co., Ltd. All bacterial-culture related reagents were purchased from Sangon Biotech (Shanghai) Co., Ltd. CB[6],[33] and MNS[34] synthesis has been reported previously and the details are shown in the Supporting Information (SI). α/β/γ-CD and fluorescent indicators rhodamine B (RhB), butyl fluorescein (BF), and 1-pyrenebutyric acid (PBA) were purchased from Sigma-Aldrich. Synthesis of benzimidazole fluorescein (BMF) is available in SI. Phosphate buffer (PB, 5 mM, pH 7.2) was used throughout.

**Sensor Array Preparation.** R1 was pristine MNSs. Thiol-modified CB[6][35] and α,β,γ-CD[36] synthesis have been reported

previously and the details are shown in SI. The host molecules modified MNSs (R2−R5): 10 mL of aqueous MNSs at 2 mg/mL was dispensed into a round-bottomed flask, 10 mg of thiol-modified host molecules was dissolved in 5 mL Millipore H₂O, and then added to the flask containing MNSs at nitrogen, and the mixture was stirred for 24 h under nitrogen atmosphere. After 24 h, excess ligands were removed by dialysis in water.[32]

**Fluorescence Titration.** The fluorescence titration of host−guest interactions between host molecules and fluorescence indicators was performed in RF-5301PC spectrophotometer (Shimadzu Scientific Instruments Inc. Tokyo, Japan). The change of indicator's fluorescence intensity was measured with increased concentration of host molecules, and the Benesi−Hildebrand equation was employed to estimate the binding constant ($K_S$). Fluorescence titration between receptor units (R1−R5) and fluorescence indicators was conducted in 96-well plates (Corning black bottom microplate) with a TriStar LB 941 microplate reader (Berthold Technologies GmbH & Co. KG, Bad Wildbad, Germany) equipped with a xenon lamp excitation source. During the titration, increased concentration of R1−R5 was added against constant fluorescent indicator concentration at 120 μL total fluid volume. Optimal concentration of R1−R5 was determined by evaluating fluorescence responses at 50−70% fluorescence quenching degree.

**Amino Acid Response.** In 96-well plates, 60 μL fluorescent indicators mixed with 24 μL R1−R5 respectively, and supplemented with 6 μL PB buffer (5 mM, pH = 7.2) first. Then, the mixture was incubated in an incubation shaker for 30 min (room temperature, 150 r/min). Next, 30 μL of standard amino acids were added to produce a total volume of 120 μL/well, with final concentration of 500 μM. For control wells, 30 μL PB was added instead of amino acid. The final mixture equilibrated for another 30 min in incubation shaker (room temperature, 150 r/min) before reading. Each amino acid was repeatedly implemented six times as described above and further used for linear discriminant analysis (LDA). In all cases, fluorescence changes reported were in reference to the control samples. The change in fluorescence intensity was used as the output response. The raw data training matrix was processed using LDA in SPSS 19.0 program.

**PG Response.** For simulated PG recognition, we designed a set of samples with different percentages of amino acids at different total concentration which simulated actual PG by using 5 common amino acids (L-Ala, D-Glu, L-Lys, D-Ala, Gly) in a bacterial cell wall PG structure. As far as the bacterial PG recognition and biosynthesis monitoring, the details of PG samples obtained are shown in SI. The fluorescence response and LDA of both simulated and bacterial PG were implemented with the same procedure as standard amino acids.

**Unknown Identification.** For detection of the unknown, amino acids and PG samples were prepared and tested using the same procedures as the training matrix. We replicated each unknown sample
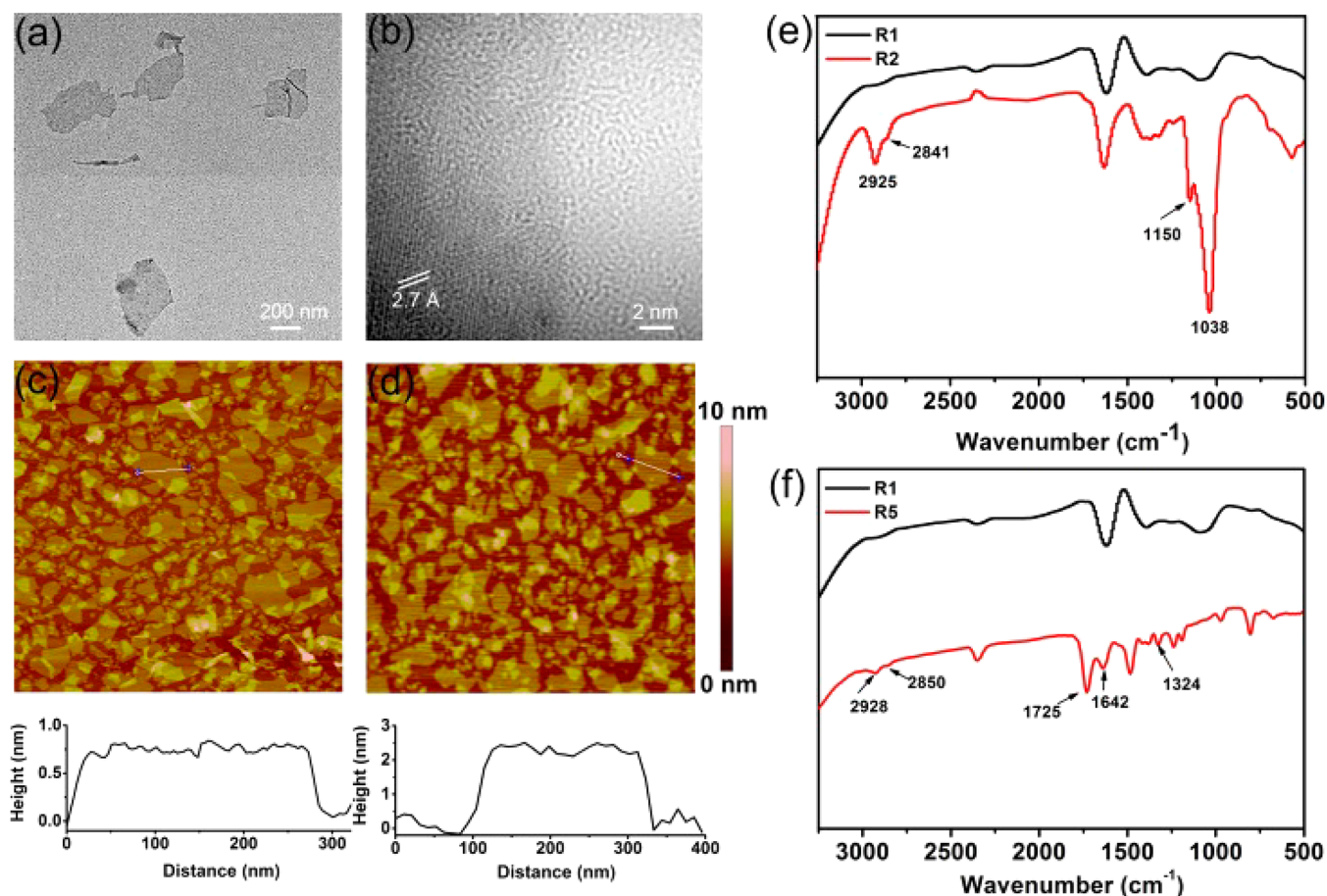
**Figure 2.** Characterizations of receptor units. (a) TEM images of R1; (b) High-resolution TEM image of layered MoS$_2$; AFM micrograph and height profile of R1 (c); R2 (d); Fourier transform infrared spectroscopy of $\alpha$-CD (e) and CB[6] (f) modified MNS.

four times, and the resulting fluorescence response patterns were subjected to LDA and were ranked in terms of their Euclidean distances to the groups generated through the training matrix and returned the nearest samples to the respective groups.

## RESULTS AND DISCUSSION

The three types of receptors consisted of five units (Figure 1b), pristine MNSs (R1) and multitypes of host molecules (i.e., $\alpha$/$\beta$/$\gamma$-CD and CB[6]) covalently modified MNSs (R2-R5). For R1, the MNSs were used as both a recognition element and a fluorescence quencher, while for R2−R5, the MNSs were used as fluorescence quencher and scaffolds. The pristine MNSs were prepared by chemical exfoliation as previously reported.[34] We first used transmission electron microscopy (TEM) and AFM to characterize MNSs morphologies before and after host molecule modification prior to use. TEM studies showed that the average size of MNSs was ca. 300 nm (Figure 2a) and the corresponding high-resolution image (Figure 2b) showed the clear hexagonal lattice structure formed by Mo and S atoms with a lattice spacing of 2.7 Å. AFM imaging (Figure 2c) showed that the layered MNSs were well-dispersed and the thinnest sheets exhibited an average height of 0.8 nm, evidencing the successful synthesis of monolayer MNSs.[32] After modification with host molecules, the thickness of the monolayer MNSs increased to ca. 2.4 nm (R2−R4, $\alpha$/$\beta$/$\gamma$-CD modified MNSs, Figure 2d and Figure S1a-b) and 2.0 nm (R5, CB[6] modified MNSs, Figure S1c), respectively. The increased height compared with pristine monolayer MNSs was due to the modification of host molecules on two sides of

the sheets which coincided with the size of host molecules (the thickness of $\alpha$/$\beta$/$\gamma$-CD is ca. 8 Å; CB[6] is ca. 6 Å), thus suggesting that the host molecules have been modified to MNSs successfully. The AFM results of R2−R5 also showed that the sheets were well-dispersed, illustrating that the modification of host molecules on MNSs did not cause aggregation of sheets, which was also confirmed by the results from TEM images (Figure S2a-d).

Fourier transform infrared spectroscopy was further used to validate the successful modification of host molecules on MNSs (Figure 2e,f and Figure S3). The presence of the host molecules was first validated by the saturated C−H stretch vibration absorption at 2839−2850 cm$^{-1}$ and 2925−2929 cm$^{-1}$. Here, the absorption present in R2−R5 but absent in R1 illustrated the presence of the host molecules. Then, the types of host molecules were validated by some unique absorption bands. For example, the secondary alcohol at 1146−1151 cm$^{-1}$ and primary alcohol at 1034−1038 cm$^{-1}$ in R2−R4 suggested the presence of D-glucose units, which revealed that CDs successfully bound to MNSs. C=O band at 1725 cm$^{-1}$, tertiary amides at 1642 cm$^{-1}$, and tertiary amine at 1324 cm$^{-1}$ present in R5 combined with C−H stretch vibration absorption, suggesting the presence of bis(methylene)-bridged glycoluril units, which demonstrated the successful modification of MNSs with CB[6].

Once the sensor array was constructed and characterized, fluorescence titration was carried out to study the host−guest interaction between host molecules and fluorescent indicators.
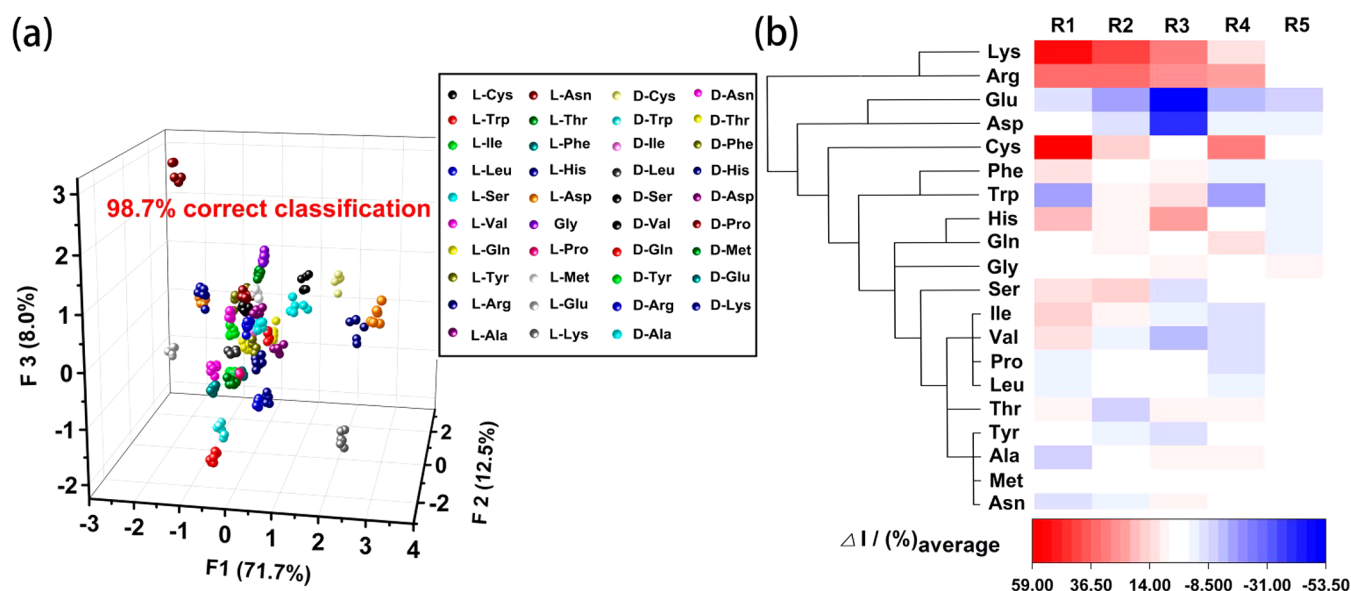
**Figure 3.** (a) LDA canonical score plot for the fluorescence response of the sensors array to 39 amino acids (19 L-amino acids, 19 D-amino acids, and Gly, all at 500 μM). (b) Heat map of the fluorescence response patterns of R1−R5 against the 20 amino acids (19 L-amino acids and Gly) and hierarchical clustering of 120 cases of 20 amino acids performed by using average linkage method (between groups).

As shown in Figure S4a-d, the fluorescence intensity of indicators changed with increased concentration of paired host molecules (Figure 1b) providing evidence of host−guest interaction. Besides, binding constants ($K_S$) between all host molecules and fluorescent indicators were calculated based on fluorescence titration (Table S1). For each host molecule, there existed a variation in binding constants among different indicators. However, the host molecule−indicator pairs (α-CD-BF, β-CD-PBA, γ-CD-RhB, CB[6]-BMF) we chose possessed the highest value, suggesting classic host−guest interactions compared with other cases. Their interaction modes, n-butyl moiety of BF, pyrene moiety of PBA, benzene lactone moiety of RhB, and benzimidazole moiety of BMF, can be effectively recognized by α-CD, β-CD, γ-CD, and CB[6], respectively, which have been reported previously.[28,37−39] To further understand the host−guest interaction modes of host molecule−indicator pairs, the feasibility that host molecules interacted with indicators was examined by using molecular mechanics/generalized Born surface area (MM/GBSA) calculations, and the details are presented in Figure S5.

From these calculations, n-butyl moiety of BF, pyrene moiety of PBA, benzene lactone moiety of RhB, and benzimidazole moiety of BMF were placed inside the α-CD, β-CD, γ-CD, and CB[6] cavities, respectively, which were found to be quite feasible (with $\Delta_{GMM-GBSA}$ = −57.8, −64.4, −86.9, and −22.1 kcal mol$^{-1}$, respectively). The interaction modes of computational results were consistent with literature reported.[28,37−39] The fluorescence titration and computational calculation results demonstrate that the fluorescent indicators we chose were reasonable and effective for indicator displacement strategy in our array sensing.

The fluorescence quenching ability of MNSs was evaluated via fluorescence titration by using RhB. The interaction of RhB with MNSs was found to be hydrophobic in nature as reported previously.[40] With increasing concentration of MNSs, the fluorescence intensity of RhB gradually decreased (Figure S4e); in the presence of 40 μg mL$^{-1}$ MNSs, the emission of RhB quenched 96% almost to the baseline level, suggesting the excellent fluorescence quenching ability of MNSs. In order to choose optimal concentration of receptors R1−R5 for sensing by plate reading, we also carried out fluorescence titration with the constant concentration of indicators. The fluorescence of indicators was quenched significantly for all receptor units, and the change of fluorescence intensity against increasing concentration of receptors (R1−R5) was plotted as Figure S6. According to fluorescence titration, we chose R1−R5 concentration for sensing when fluorescence intensity decreased 50−70% but was not totally quenched in the consideration of two aspects. On one hand, with the addition of analytes, the fluorescence was most commonly recovered due to competitive displacement of the fluorescent reporters. Thus, the 50−70% quenching rate allowing a fluorescent recovery space. One the other hand, there were also some instances of further fluorescent quenching due to the change of chemical environment after analyte addition and the resulting aggregation and self-quenching of fluorescent reporters,[41] or due to the charge transfer from the reporters to the analyte through noncovalent interactions such as electrostatic and hydrophobic interactions, which induced further quenching.[42,43] Therefore, the moderate 50−70% quenching points allowing a signal readout for the aforementioned cases. The optimal concentration of R1−R5 and corresponding fluorescent indicators or sensor array in our work were listed in Table S2 and used for array sensing throughout.

To validate the potential efficiency of our sensor array for monitoring of PG biosynthesis, we first performed tests to identify standard amino acids with respect to chirality. The discriminant ability of our sensor array for a considerable amount of chiral amino acids was verified by discriminating 39 amino acids including 19 L-amino acids and the corresponding 19 D-enantiomers as well as the achiral Gly. LDA was used to differentiate quantitatively the fluorescence response patterns of 39 amino acids against five receptor units R1−R5.[44] In LDA, the "memory" or "training matrix" was generated using "known samples" that maximized the ratio of between-class variance to within-class variance, which thus allowed response patterns to
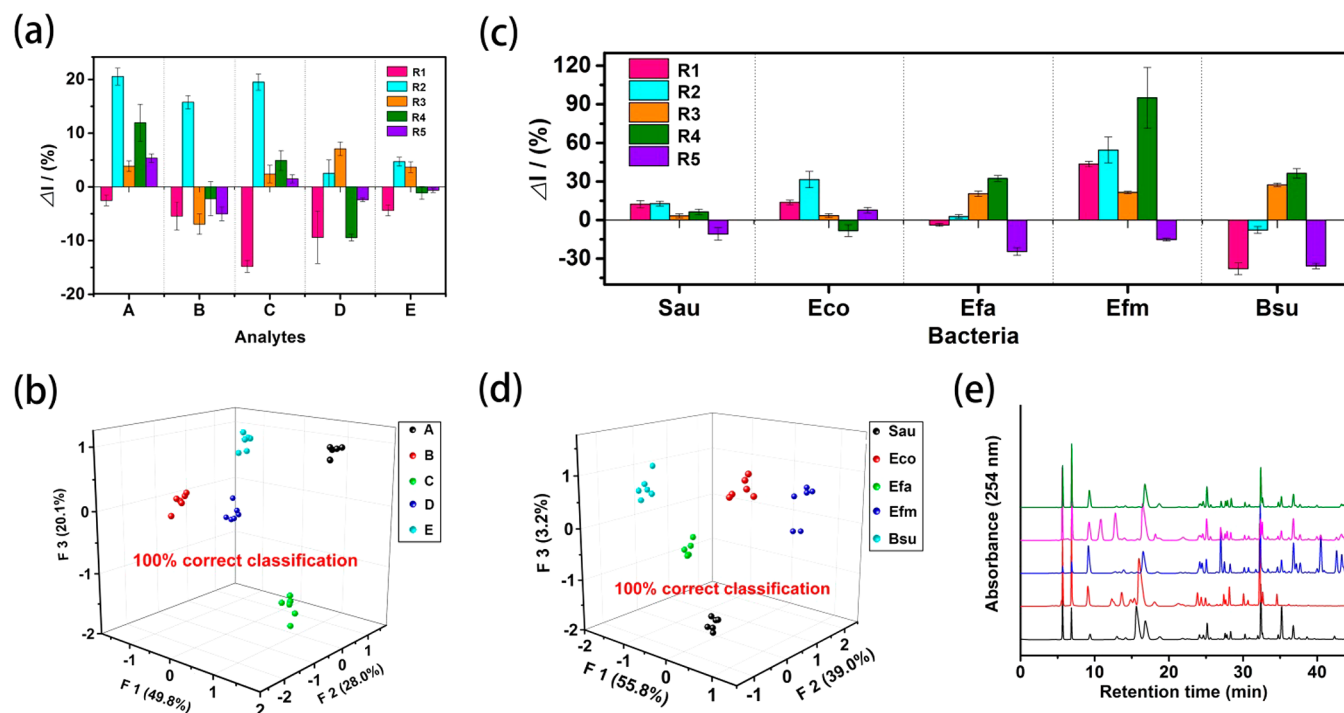
**Figure 4.** (a) Fluorescence response patterns of R1−R5 against simulated PG samples A−E (A−E explained as Table S14). (b) LDA canonical score plot for the fluorescence response of the sensors array to simulated PG sample A−E. (c) Fluorescence response patterns of R1−R5 against five bacterial PG. (d) LDA canonical score plot for the fluorescence response of the sensor arrays to five bacterial PG. (e) Chromatographic analysis of amino acid composition of PG purified from different species of bacteria. Black, Sau; red, Efa; blue, Bsu; magenta, Efm; green, Eco.

be differentiated. Based on this principle, we used LDA to produce four canonical factors (71.7%, 12.5%, 8.0%, and 7.8%) from the fluorescence response patterns (5 receptor units × 39 amino acids × 6 replicates, Figure S7 and Table S3). The canonical factors represent linear combinations of the response matrices. The 234 training cases (39 amino acids × 6 replicates) were distinguished as 39 respective groups with 98.7% accuracy. The top three factors were plotted in a 3D model (Figure 3a), and some amino acids were partly overlapped due to the angle of view. After locally magnifying Figure 3a and rotating it with a certain angle, the overlapped amino acids can be obviously distinguished (Figure S8). The chiral recognition efficiency was validated by the identification of 156 randomly unknown cases from our training matrix. Only 10 samples were incorrectly identified, which indicates a 93.6% accuracy (Table S4).

Herein, the successful enantioselective sensing should be attributed to chiral selectivity of the three α-, β-, and γ-CDs. As previously reported, hydrophobic groups of a compound with proper size can insert into the hydrophobic cavity of CDs. Besides, hydrophilic groups such as amino and carboxyl can interact with the hydroxyls (−OH) on the outer rims of CDs via H-bonding and other noncovalent interactions. Due to the multiple chiral centers in CDs, both the hydrophobic inclusions and hydrophilic interactions are all enantioselective, endowing the CDs with potent chiral recognition capability.[45,46] Thus, we determined the binding constants between different amino acid enantiomers and host molecules by UV−vis spectrometric titration. As shown in Table S5, many enantiomeric amino acids associate with CDs significant differently, and α/β/γ-CD associate with a certain amino acid with different binding constants. Thus, these above differences provide the possibility

of our constructed sensor array to discriminate a variety of amino acid enantiomers.

The discrimination ability of the amino acid species of our sensor array to ignore chirality was remarkable, because there were far more discriminated amino acid species in our work than in other arrays reported previously.[47] According to the fluorescence response patterns from Figure S7 the species discriminant accuracy was 100% in training trials of both L- and D-amino acids (Figure S9), and 95% in unknown L-amino acids and 96.1% in unknown D-amino acids (Table S6 and Table S7). Thus, the sensor array we designed showed effective chiral recognition ability in addition to conventional amino acid species discrimination.

Surprisingly, effective chiral amino acid identification was possible even using simple Euclidean distances, which only compared the overall total response of the array. Euclidean described the distance and similarity between each of the 234 individual cases. Figure S10 showed that the Euclidean distance between each of the six replicates of an amino acid was similar, while it varied among different species of amino acids, which suggested the possibility to classify 234 cases correctly.

More accurate chiral recognition was demonstrated by discriminating enantiomeric purity by only using R2−R4 which contain chiral cavities in the host α/β/γ-CD molecules. This was carried out by taking Ile as an example. In LDA results (Figure S11), 36 training cases (6 enantiomeric purity × 6 replicates, Table S8) of Ile could be discriminated completely in initial trials and only one unknown case was misclassified, affording a classification accuracy of 95.8% (Table S9). Therefore, our sensor array exhibited excellent chiral recognition ability.

In addition to chiral recognition, our sensor array was sufficiently sensitive to identify changes of amino acid
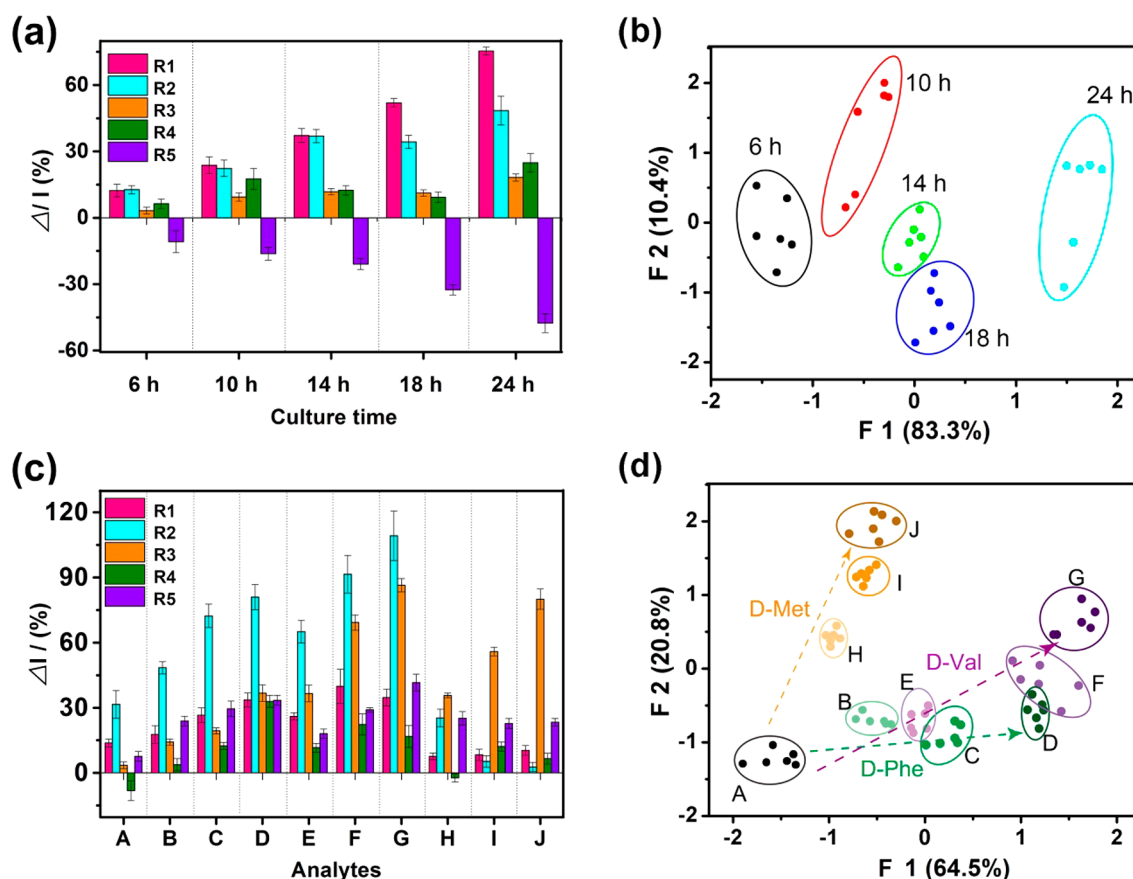
**Figure 5.** Monitoring of PG biosynthesis with sensor array constructed with R1−R5. (a) Fluorescence response patterns of R1−R5 against five PG samples from different culture times of Sau. (b) LDA canonical score plot for the fluorescence response of the sensor array to five PG samples from different culture times of Sau with accuracy of 100% and 95% confidence ellipses. (c) Fluorescence response patterns of R1−R5 against PG samples from different D-amino acid cultured Eco: A, normal cultured; B, normal cultured with addition of 10 μM D-Phe before sensing; C, normal cultured with addition of 100 μM D-Phe before sensing; D, cultured with 20 mM D-Phe; E, normal cultured with addition of 10 μM D-Val before sensing; F, normal cultured with addition of 100 μM D-Val before sensing; G, cultured with 20 mM D-Val; H, normal cultured with addition of 10 μM D-Met before sensing; I, normal cultured with addition of 100 μM D-Met before sensing; J, cultured with 20 mM D-Met. (d) LDA canonical score plot for the fluorescence response of the sensors array to PG samples from different D-amino acid cultured Eco with accuracy of 98.3% and 95% confidence ellipses; letters (A−J) are the same as in part c.

concentration. As demonstrated, L-Trp was chosen as the model and the fluorescence response patterns of different concentration were shown in Figure S12a. The 36 training cases (6 concentrations × 6 replicates, Table S10) could be assigned to their respective groups with 100% accuracy using LDA (Figure S12b). Of 24 unknown cases, 23 were correctly classified, affording an identification accuracy of 95.8% (Table S11). As shown in Figure S12c, the linearity of the dose−response curve for L-Trp suggested that the interactions between R1−R5 and amino acids were stable and the sensor array was highly reproducible.

To quantify the amino acid in the mixture containing several amino acids, we designed a mixture containing five amino acids, including L-Ala, D-Ala, L-Lys, D-Glu, and Gly (each at a concentration of 2 μM) which are common components in bacterial peptidoglycan. Then, D-Phe with different concentration ranges from 0 to 8.0 μM was added to the mixture, and analyzed by our sensor array. The fluorescence response patterns and LDA canonical score plot of the sensor array to different concentrations of D-Phe in mixture are shown in Table S12 and Figure S13, and the samples with different D-Phe concentration in the mixture could be totally discriminated. Finally, we extracted canonical factor 1 (F1) as y axis and D-Phe

concentration as x axis to draw plots and fitted as linear curve with formula of $y = 0.38x − 1.29$ and linear correlation $R^2$ of 0.977. Thus, the unknown concentration of D-Phe (Table S13) in this mixture could be quantified according to the training matrix with an accuracy of 95.8%.

Furthermore, we performed hierarchical clustering analysis (HCA) to validate that the results from our sensor array were scientific and effective. Unlike LDA, HCA is a model-free standard chemometric approach to cluster similar subjects into a group based on their spatial distances in full vector space.[48] We took the average fluorescence response of each species of amino acid (19 L-amino acids and Gly) to perform HCA and drew the heat map as Figure 3b. The differential response pattern in the heat map demonstrated the high sensitivity of the sensor array to different amino acids. HCA produced several classes, which was consistent with the physicochemical properties of amino acids such as polarity and charge. For example, L-Lys and L-Arg were classified as a class since they were polar and positive amino acids, L-Phe and L-Trp, in a class since they were amino acids with benzene ring, L-Ile/Val/Pro/Leu in a class as they were hydrophobic amino acids, and L-Cys was sui generis due to its unique thiol. The results of HCA

indicated that the sensor array we constructed was scientific, effective, and reflected the intrinsic properties of analytes.

We next investigated the amino acid mixture that simulated PG compositions (Table S14) to validate that the recognition ability of our sensor array was not sacrificed in complex mixtures. The training samples A to E (Figure 4a and Table S15) were clearly distinguished from each other in the LDA plot with the accuracy of 100% (Figure 4b). Amazingly, all the unknown stimulated PG samples were correctly classified (Table S16), which indicated that our constructed sensor array showed excellent discriminant ability in amino acid mixtures and thus had great potential for bacterial PG recognition.

Based on this achievement, we investigated the recognition ability of our sensor array for real bacterial PG samples. The bacterial PG related amino acid composition and cross-linking of peptide stem are highly diverse among different species. Besides, the content of PG in the cell wall is also different among different species, and the PG layers in Gram-positive bacteria are always thicker than those in Gram-negative.[49] Thus, these differences provide the possibility for accurate PG recognition by using our sensor array. As demonstrated, we randomly chose four species of Gram-positive bacteria: *Staphylococcus aureus* (Sau), *Enterococcus faecalis* (Efa), *Enterococcus faecium* (Efm), *Bacillus subtilis* (Bsu), and one Gram-negative bacteria *Escherichia coli* (Eco) as the model objects. Their amino acid composition and cross-linking of the peptide stem listed in Table S17 indicated that there was a discrepancy in both the composition and cross-linking of the peptide stem.[2,50−52] After performing the same sensing procedures as above, the fluorescence response patterns (Figure 4c and Table S18) of five bacterial PG were subjected to LDA, and consequently four canonical factors (55.8%, 39.0%, 3.2%, and 2.0%) were produced. The top three factors were presented in Figure 4d. The discrimination accuracy was 100% in both 30 training cases and 20 unknown trials (Table S19). To illustrate that accurate discriminant of PG by our constructed sensor array was related to PG amino acids composition, we conducted HPLC analysis of PG after acid hydrolysis and tosyl amide derivatization as shown in Figure 4e. There were differences in composition of eluent among bacterial species for the different retention time and peak intensity. The HPLC results proved the accuracy of our fluorescence response pattern-based array sensing (Figure 4c). Hence our sensor array was demonstrated to be a powerful tool for PG's amino acid composition analysis, and the bacterial species could be correctly identified through PG recognition.

Successful PG recognition of different bacterial species made it possible to monitor dynamic PG composition during cell wall biosynthesis using the constructed sensor array. We took Sau as an example to validate that the array could monitor the change of PG along with growth phase. We obtained five PG samples at culture times of 6, 10, 14, 18, and 24 h respectively according to the growth curve of Figure S14. The fluorescence response pattern and score plot of the first two factors produced from LDA with 95% confidence ellipses were presented in Figure 5a,b. Discriminant accuracy of 30 original trials (5 samples × 6 replicates, Table S20) about different growth stages of Sau reached 100%. We next tested the array against unknowns taken from the training set. Out of 30 samples, 27 were identified correctly, which gives a 90% identification accuracy (Table S21), even though there were only subtle differences among different culture times as HPLC analysis showed in Figure S15a. The peak area ratio of Gly/Ala decreased with

extension of culture time, which was ascribed to the depletion of Gly in the nutrient medium and the lack of attached penta-Gly bridges for part of the PG stems in stationary phases.[3] In addition, there existed a trend in PG biosynthesis (Figure 5b) that PG samples with longer culture time got higher F1 score with the distribution of PG sample plots more closed to the right. These results suggested that the proposed array allows us to monitor dynamic subtle changes of PG composition during bacterial growth and thus identify the growth stage of bacteria based on their PG composition changes.

Furthermore, we also verified the ability of our sensor array to monitor the chiral changes in PG biosynthesis caused by incorporation of exogenous D-amino acids. In this work, three types of D-amino acids including D-Met, D-Phe, and D-Val were added during Eco culture and their concentration was controlled at 20 mM, which did not affect the growth of bacteria as reported previously.[6] To demonstrate that exogenous D-amino acids were incorporated into PG structure, the PG samples were also collected from normally cultured Eco without any addition and then the three aforementioned D-amino acids with known concentrations were added before sensing as control trials. The fluorescence response pattern (Figure 5c and Table S22) of all the above samples was subjected to LDA, and then the canonical score plot (Figure 5d) was obtained based on the first two factors with 95% confidence ellipses. The LDA results showed that the PG patterns could be accurately differentiated, and only one PG sample (Eco cultured with 20 mM D-Phe) was misclassified, affording an accuracy of 98.3%. For 40 unknown PG samples obtained as training trials, only four samples were incorrectly identified, affording an identification accuracy of 90% (Table S23).

Figure 5d explained how the exogenous D-amino acids affected PG biosynthesis from a new point of view. The black ellipse A was taken as the originally represented PG samples from Eco normally cultured without any D-amino acid addition. The ellipses at the ends of the three arrows were PG samples from Eco cultured with 20 mM D-amino acids (D: Phe; G: Val; J: Met). Between ellipse A and D, there were two ellipses representing PG samples from normal cultured Eco added with corresponding standard D-Phe before sensing with final concentration of 10 μM (ellipse B) and 100 μM (ellipse C). Ellipses A to D indicated that with higher concentration of added standard D-Phe, the obtained F1 score was higher, and the ellipse C with highest concentration of D-Phe was close to the ellipse D located at the end of green arrow that represent Eco cultured with 20 mM D-Phe. This arrow indicated that the PG sample of ellipse D contained D-Phe. Similar trends were also observed for the cases of D-Val and D-Met. These arrows demonstrated that the impact of D-amino acids on bacterial PG structure was indeed due to the incorporation of D-amino acids. The result was in accordance with HPLC results (Figure S15b) that PG from Eco cultured with exogenous D-amino acids produced corresponding D-amino acids in their peptide stems, indicating the reliability of the proposed chiral sensor array.

## ■ CONCLUSIONS

In summary, we developed a novel chiral sensor array based on multitypes of host molecule modified MNSs. Due to the combination of multiple host−guest interactions, the sensor array can obtain more information on analytes such as chirality, polarity, charge, and size at the same time, and thus achieve the enormous improvement in its recognition ability. The array

enables accurate chiral recognition of amino acids besides their species identification. Significantly, this approach also allowed the identification of bacterial species via PG recognition at a new point of view. Furthermore, the sensor has been proven effective in monitoring PG biosynthesis under different growth stages and nutritional conditions even though only a subtle change existed in the PG structure. Compared to the conventional sensor arrays, the chiral sensor array we constructed was facile, accurate, and robust, and thus holds great promise for potential applications in environmental safety, microbial physiology, and biomedical research.

## ■ ASSOCIATED CONTENT

### Ⓢ Supporting Information

The Supporting Information is available free of charge on the ACS Publications website at DOI: 10.1021/acssensors.7b00676.

> Experimental details; Characterizations of receptor units; Study on the interaction between receptor units and indicators; Figures of array sensing; Growth curves of five bacteria; Chromatographic analysis of PG samples; Fluorescence titration results; Raw data of array sensing (PDF)

## ■ AUTHOR INFORMATION

### Corresponding Author

*E-mail: wlwei@cqu.edu.cn.

### ORCID Ⓘ

Weili Wei: 0000-0001-6363-3591

### Notes

The authors declare no competing financial interest.

## ■ ACKNOWLEDGMENTS

## ■ REFERENCES

(1) Schleifer, K. H.; Kandler, O. Peptidoglycan types of bacterial cell walls and their taxonomic implications. *Bacteriol Rev.* **1972**, *36*, 407−477.

(2) Vollmer, W.; Blanot, D.; de Pedro, M. A. Peptidoglycan structure and architecture. *FEMS Microbiol. Rev.* **2008**, *32*, 149−167.

(3) Zhou, X.; Cegelski, L. Nutrient-dependent structural changes in *S. aureus* peptidoglycan revealed by solid-state NMR spectroscopy. *Biochemistry* **2012**, *51*, 8143−8153.

(4) Vijaranakul, U.; Nadakavukaren, M. J.; de Jonge, B. L.; Wilkinson, B. J.; Jayaswal, R. K. Increased Cell Size and Shortened Peptidoglycan Interpeptide Bridge of NaCl-Stressed *Staphylococcus aureus* and Their Reversal by Glycine Betaine. *J. Bacteriol.* **1995**, *177*, 5116−5121.

(5) Takacs, C. N.; Hocking, J.; Cabeen, M. T.; Bui, N. K.; Poggio, S.; Vollmer, W.; Jacobswagner, C. Growth Medium-Dependent Glycine Incorporation into the Peptidoglycan of Caulobacter Crescentus. *PLoS One* **2013**, *8*, e57579.

(6) Caparrós, M.; Pisabarro, A. G.; de Pedro, M. A. Effect of D-amino Acids on Structure and Synthesis of Peptidoglycan in *Escherichia coli. J. Bacteriol.* **1992**, *174*, 5549−5559.

(7) Mainardi, J. L.; Villet, R.; Bugg, T. D.; Mayer, C.; Arthur, M. Evolution of Peptidoglycan Biosynthesis Under the Selective Pressure of Antibiotics in Gram-Positive Bacteria. *FEMS Microbiol.Rev.* **2008**, *32*, 386−408.

(8) Lam, H.; Waldor, M. K. D-amino Acids Govern Stationary Phase Cell Wall Remodeling in Bacteria. *Science* **2009**, *325*, 1552−1555.

(9) Bugg, T. D. Biosynthesis: Imaging Cell-Wall Biosynthesis live. *Nat. Chem.* **2013**, *5*, 10−12.

(10) Scheffers, D. J.; Pinho, M. G. Bacterial Cell Wall Synthesis: New Insights from Localization Studies. *Microbiol. Mol. Biol. Rev.* **2005**, *69*, 585−607.

(11) Boneca, I. G. The Role of Peptidoglycan in Pathogenesis. *Curr. Opin. Microbiol.* **2005**, *8*, 46−53.

(12) Bugg, T. D.; Walsh, C. T. Intracellular Steps of Bacterial Cell Wall Peptidoglycan Biosynthesis: Enzymology, Antibiotics, and Antibiotic Resistance. *Nat. Prod. Rep.* **1992**, *9*, 199.

(13) Desmarais, S. M.; de Pedro, M. A.; Cava, F.; Huang, K. C. Peptidoglycan at its Peaks: How Chromatographic Analyses Can Reveal Bacterial Cell-Wall Structure and Assembly. *Mol. Microbiol.* **2013**, *89*, 1−13.

(14) Turner, R. D.; Hurd, A. F.; Cadby, A.; Hobbs, J. K.; Foster, S. J. Cell Wall Elongation Mode in Gram-Negative Bacteria is Determined by Peptidoglycan Architecture. *Nat. Commun.* **2013**, *4*, 1496.

(15) Gan, L.; Chen, S.; Jensen, G. J. Molecular Organization of Gram-Negative Peptidoglycan. *Proc. Natl. Acad. Sci. U. S. A.* **2008**, *105*, 18953−18957.

(16) Schiller, A.; Wessling, R. A.; Singaram, B. A Fluorescent Sensor Array for Saccharides Based on Boronic Acid Appended Bipyridinium Salts. *Angew. Chem., Int. Ed.* **2007**, *46*, 6457−6459.

(17) Mrinmoy, D. E.; Rana, S.; Akpinar, H.; Miranda, O. R.; Arvizo, R. R.; Bunz, U. H. F.; Rotello, V. M. Sensing of Proteins in Human Serum using Nanoparticle-Green Fluorescent Protein Conjugates. *Nat. Chem.* **2009**, *1*, 461−465.

(18) Bajaj, A.; Miranda, O. R.; Phillips, R.; Kim, I.-B.; Jerry, D. J.; Bunz, U. H. F.; Rotello, V. M. Array-Based Sensing of Normal, Cancerous, and Metastatic Cells Using Conjugated Fluorescent Polymers. *J. Am. Chem. Soc.* **2010**, *132*, 1018−1022.

(19) Carey, J. R.; Suslick, K. S.; Hulkower, K. I.; Imlay, J. A.; Imlay, K. R. C.; Ingison, C. K.; Ponder, J. B.; Sen, A.; Wittrig, A. E. Rapid Identification of Bacteria with a Disposable Colorimetric Sensing Array. *J. Am. Chem. Soc.* **2011**, *133*, 7571−7576.

(20) Lim, S. H.; Feng, L.; Kemling, J. W.; Musto, C. J.; Suslick, K. S. An Optoelectronic Nose for the Detection of Toxic Gases. *Nat. Chem.* **2009**, *1*, 562−567.

(21) Rana, S.; Le, N. D.; Mout, R.; Saha, K.; Tonga, G. Y.; Bain, R. E.; Miranda, O. R.; Rotello, C. M.; Rotello, V. M. A Multichannel Nanosensor for Instantaneous Readout of Cancer Drug Mechanisms. *Nat. Nanotechnol.* **2015**, *10*, 65−69.

(22) Peng, G.; Tisch, U.; Adams, O.; Hakim, M.; Shehada, N.; Broza, Y. Y.; Billan, S.; Abdah-Bortnyak, R.; Kuten, A.; Haick, H. Diagnosing Lung Cancer in Exhaled Breath using Gold Nanoparticles. *Nat. Nanotechnol.* **2009**, *4*, 669−673.

(23) Rana, S.; Singla, A. K.; Bajaj, A.; Elci, S. G.; Miranda, O. R.; Mout, R.; Yan, B.; Jirik, F. R.; Rotello, V. M. Array-Based Sensing of Metastatic Cells and Tissues using Nanoparticle-Fluorescent Protein Conjugates. *ACS Nano* **2012**, *6*, 8233−8240.

(24) Yu, G.; Jie, K.; Huang, F. Supramolecular Amphiphiles Based on Host-Guest Molecular Recognition Motifs. *Chem. Rev.* **2015**, *115*, 7240−7303.

(25) Ma, X.; Zhao, Y. Biomedical Applications of Supramolecular Systems Based on Host-Guest Interactions. *Chem. Rev.* **2015**, *115*, 7794.

(26) Peng, H. Q.; Niu, L. Y.; Chen, Y. Z.; Wu, L. Z.; Tung, C. H.; Yang, Q. Z. Biological Applications of Supramolecular Assemblies Designed for Excitation Energy Transfer. *Chem. Rev.* **2015**, *115*, 7502−7542.

(27) Szente, L.; Szemán, J. Cyclodextrins in Analytical Chemistry: Host-Guest Type Molecular Recognition. *Anal. Chem.* **2013**, *85*, 8024−8030.

(28) Harada, A.; Kobayashi, R.; Takashima, Y.; Hashidzume, A.; Yamaguchi, H. Macroscopic Self-Assembly Through Molecular Recognition. *Nat. Chem.* **2011**, *3*, 34−37.

(29) Barrow, S. J.; Kasera, S.; Rowland, M. J.; del Barrio, J.; Scherman, O. A. Cucurbituril-Based Molecular Recognition. *Chem. Rev.* **2015**, *115*, 12320−12406.

(30) Zhu, C.; Zeng, Z.; Li, H.; Li, F.; Fan, C.; Zhang, H. Single-Layer MoS$_2$-Based Nanoprobes for Homogeneous Detection of Biomolecules. *J. Am. Chem. Soc.* **2013**, *135*, 5998−6001.

(31) Perkins, F. K.; Friedman, A. L.; Cobas, E.; Campbell, P. M.; Jernigan, G. G.; Jonker, B. T. Chemical Vapor Sensing with Monolayer MoS$_2$. *Nano Lett.* **2013**, *13*, 668−673.

(32) Chou, S. S.; De, M.; Kim, J.; Byun, S.; Dykstra, C.; Yu, J.; Huang, J.; Dravid, V. P. Ligand Conjugation of Chemically Exfoliated MoS$_2$. *J. Am. Chem. Soc.* **2013**, *135*, 4584−4587.

(33) Kim, J.; Jung, I. S.; Kim, S. Y.; Lee, E.; Kang, J. K.; Sakamoto, S.; Yamaguchi, K.; Kim, K. New Cucurbituril Homologues: Syntheses, Isolation, Characterization, and X-ray Crystal Structures of Cucurbit-[n]uril (n = 5, 7, and 8). *J. Am. Chem. Soc.* **2000**, *122*, 540−541.

(34) Matte, H. S.; Gomathi, A.; Manna, A. K.; Late, D. J.; Datta, R.; Pati, S. K.; Rao, C. N. MoS$_2$ and WS$_2$ Analogues of Graphene. *Angew. Chem., Int. Ed.* **2010**, *49*, 4059−4062.

(35) Cui, S. C.; Tachikawa, T.; Fujitsuka, M.; Majima, T. Photoinduced Electron Transfer in a Quantum Dot−Cucurbituril Supramolecular Complex. *J. Phys. Chem. C* **2011**, *115*, 1824−1830.

(36) Jing, B.; Chen, X.; Wang, X.; Zhao, Y.; Qiu, H. Sol-Gel-Sol Transition of Gold Nanoparticle-Based Supramolecular Hydrogels Induced by Cyclodextrin Inclusion. *ChemPhysChem* **2008**, *9*, 249−252.

(37) Xu, W.; Demas, J. N.; Degraff, B. A.; Whaley, M. Interactions of Pyrene with Cyclodextrins and Polymeric Cyclodextrins. *J. Phys. Chem.* **1993**, *97*, 6546−6554.

(38) Ding, Y.; Zhu, H.; Zhang, X.; Zhu, J. J.; Burda, C. Rhodamine B Derivative-Functionalized Upconversion Nanoparticles for FRET-Based Fe$^{3+}$-Sensing. *Chem. Commun.* **2013**, *49*, 7797−7799.

(39) Ge, J. Y.; Xue, S. F.; Zhu, Q. J.; Tao, Z.; Zhang, J. X. Interaction of Cucurbit[n = 6 ∼ 8]urils and Benzimidazole Derivatives. *J. Inclusion Phenom. Mol. Recognit. Chem.* **2007**, *58*, 63−69.

(40) Shakya, J.; Sahoo, H.; Mohanty, T. A study on the Interaction between Molybdenum Disulfide and Rhodamine B by Spectroscopic methods. *J. Mater. Sci.* **2017**, *52*, 3831.

(41) Chou, S. S.; De, M.; Luo, J.; Rotello, V. M.; Huang, J.; Dravid, V. P. Nanoscale Graphene Oxide (nGO) as Artificial Receptors: Implications for Biomolecular Interactions and Sensing. *J. Am. Chem. Soc.* **2012**, *134*, 16725−16733.

(42) Wang, H. S.; Li, J.; Li, J. Y.; Wang, K.; Ding, Y.; Xia, X. H. Lanthanide-based Metal-organic Framework Nanosheets with Unique Fluorescence Quenching Properties for Two-color Intracellular Adenosine Imaging in Living Cells. *NPG Asia Mater.* **2017**, *9*, e354.

(43) Wang, H. S.; Bao, W. J.; Ren, S. B.; Chen, M.; Wang, K.; Xia, X. H. Fluorescent sulfur-tagged europium(iii) coordination polymers for monitoring reactive oxygen species. *Anal. Chem.* **2015**, *87*, 6828−6833.

(44) Jurs, P. C.; Bakken, G. A.; Mcclelland, H. E. Computational Methods for the Analysis of Chemical Sensor Array Data from Volatile Analytes. *Chem. Rev.* **2000**, *100*, 2649−2678.

(45) Hembury, G. A.; Borovkov, V. V.; Inoue, Y. Chirality-sensing supramolecular systems. *Chem. Rev.* **2008**, *108*, 1−73.

(46) Jin, L. J.; Rodriguez, I.; Li, S. F. Y. Enantiomeric Separation of Amino Acids Derivatized with Fluoresceine Isothiocyanate Isomer I by Micellar Electrokinetic Chromatography Using $\beta$- and $\gamma$-cyclodextrins as Chiral Selectors. *Electrophoresis* **1999**, *20*, 1538−1545.

(47) Minami, T.; Esipenko, N. A.; Zhang, B.; Isaacs, L.; Anzenbacher, P. "Turn-on" Fluorescent Sensor Array for Basic Amino Acids in Water. *Chem. Commun.* **2014**, *50*, 61−63.

(48) Scott, S. M.; James, D.; Ali, Z. Data Analysis for Electronic Nose Systems. *Microchim. Acta* **2006**, *156*, 183−207.

(49) Popham, D. L. Visualizing the Production and Arrangement of Peptidoglycan in Gram-Positive Cells. *Mol. Microbiol.* **2013**, *88*, 645−649.

(50) Steen, A.; Buist, G.; Horsburgh, G. J.; Venema, G.; Kuipers, O. P.; Foster, S. J.; Kok, J. AcmA of *Lactococcus lactis* is an N-Acetylglucosaminidase with an Optimal Number of LysM Domains for Proper Functioning. *FEBS J.* **2005**, *272*, 2854−2868.

(51) Bellais, S.; Arthur, M.; Dubost, L.; Hugonnet, J. E.; Gutmann, L.; Van Heijenoort, J.; Legrand, R.; Brouard, J. P.; Rice, L.; Mainardi, J. L. Aslfm, the D-Aspartate Ligase Responsible for the Addition of D-Aspartic Acid onto the Peptidoglycan Precursor of *Enterococcus faecium*. *J. Biol. Chem.* **2006**, *281*, 11586−11594.

(52) Bouhss, A.; Josseaume, N.; Severin, A.; Tabei, K.; Hugonnet, J. E.; Shlaes, D.; Lecreulx, D. M.; van Heijenoort, J.; Arthur, M. Synthesis of the L-Alanyl-L-Alanine Cross-Bridge of *Enterococcus faecalis* Peptidoglycan. *J. Biol. Chem.* **2002**, *277*, 45935−45941.